Scientific Reports

https://doi.org/10.1038/s41598-026-44916-4

Article in Press

Germ cells are essential for testicular morphogenesis and functional reconstruction in a porcine xenograft model

Received: 12 August 2025

Accepted: 16 March 2026

Published online: 23 March 2026

Cite this article as: Han M., Jeon Y., Maeng H. *et al.* Germ cells are essential for testicular morphogenesis and functional reconstruction in a porcine xenograft model. *Sci Rep* (2026). https://doi.org/10.1038/s41598-026-44916-4

Min-Gi Han, Yoseop Jeon, Hyoyoung Maeng, Donghyeon Kim, Jeong Tae Do, Kwonho Hong, Youngsok Choi & Hyuk Song

We are providing an unedited version of this manuscript to give early access to its findings. Before final publication, the manuscript will undergo further editing. Please note there may be errors present which affect the content, and all legal disclaimers apply.

If this paper is publishing under a Transparent Peer Review model then Peer Review reports will publish with the final article.

ARTICLE IN PRESS

© The Author(s) 2026. **Open Access** This article is licensed under a Creative Commons Attribution-NonCommercial-NoDerivatives 4.0 International License, which permits any non-commercial use, sharing, distribution and reproduction in any medium or format, as long as you give appropriate credit to the original author(s) and the source, provide a link to the Creative Commons licence, and indicate if you modified the licensed material. You do not have permission under this licence to share adapted material derived from this article or parts of it. The images or other third party material in this article are included in the article's Creative Commons licence, unless indicated otherwise in a credit line to the material. If material is not included in the article's Creative Commons licence and your intended use is not permitted by statutory regulation or exceeds the permitted use, you will need to obtain permission directly from the copyright holder. To view a copy of this licence, visit http://creativecommons.org/licenses/by-nc-nd/4.0/.

ARTICLE IN PRESS

Germ Cells Are Essential for Testicular Morphogenesis and Functional Reconstruction in a Porcine Xenograft Model

Min-Gi Han[1], Yoseop Jeon[1], Hyoyoung Maeng[1], Donghyeon Kim[1], Jeong Tae Do[1], Kwonho Hong[1], Youngsok Choi[1], and Hyuk Song[1*]

[1]Department of Stem Cells and Regenerative Technology, Konkuk University, Seoul 05029, Republic of Korea

[*]**Corresponding author:** Hyuk Song

Department of Stem Cells and Regenerative Technology, Konkuk University, Seoul 05029, Republic of Korea

Tel: +82-2-450-0562, Email: Songh@konkuk.ac.kr

Contributing author emails:

Min-Gi Han

Email: hmg82@konkuk.ac.kr

Yoseop Jeon

Email: jeonjoseph@konkuk.ac.kr

Hyoyoung Maeng

Email: mang0724@konkuk.ac.kr

Donghyeon Kim

Email: kdh2987@konkuk.ac.kr

Jeong Tae Do

Email: dojt@konkuk.ac.kr

Kwonho Hong

Email: hongk@konkuk.ac.kr

Youngsok Choi

E-mail: choiys3969@konkuk.ac.kr

ARTICLE IN PRESS

ARTICLE IN PRESS

Abstract

Reconstruction of functional testis tissue can provide new opportunities for in vitro spermatogenesis and fertility restoration in livestock. Although testis reconstruction has been reported in several species, the germ cell–dependent mechanisms underlying de novo testicular morphogenesis remain insufficiently defined in large animals.. In this study, we investigated the contribution of porcine spermatogonial stem cells (pSSCs) to testis morphogenesis and spermatogenesis using a xenograft model. Testicular cells containing approximately 10% germ cells combined with a somatic-enriched fraction (SEF) (GF group) or SEF only (FO group) were transplanted subcutaneously into immunodeficient mice and examined after six months. GF tissues developed well-organized seminiferous tubules and showed multiple spermatogenic stages, whereas FO tissues remained fragmented, poorly organized, and lacked stable tubular architecture. Immunofluorescence analyses revealed appropriate localization of germ cells and maturation-associated features of Sertoli cells in GF tissues, whereas FO tissues exhibited aberrant Sertoli cell localization and marker expression patterns. Transcriptomic profiling further showed enrichment of cell cycle– and spermatogenesis-related pathways in GF tissues, while FO tissues exhibited upregulation of coagulation-, inflammation-, and early developmental pathways, consistent with impaired tissue organization. Collectively, these findings demonstrate that pSSCs are indispensable for initiating and stabilizing testicular morphogenesis in xenograft condition and underscore the utility of this model for advancing reproductive biotechnology in livestock.

Keywords: xenograft, testicular morphogenesis, spermatogonial stem cells, testis reconstruction, porcine testis,

ARTICLE IN PRESS

ARTICLE IN PRESS

Background

Climate change has emerged as a major threat to global livestock productivity, with rising temperatures and environmental stressors impairing animal fertility and reproductive efficiency (1). To address these challenges, the development of reproductive technologies capable of forming testes and producing functional sperm *in vitro* has become increasingly critical, representing a significant area in reproductive biotechnology (2). *In vitro* spermatogenesis not only provides a powerful tool for investigating fundamental processes of germ cell development and testicular biology, but also holds considerable promise for both clinical and agricultural applications (3, 4). *In vitro* testis reconstitution, when integrated with long-term spermatogonial stem cell (SSC) culture, may contribute to continuous breeding strategies, preservation of superior genetic lines, fertility management with impaired testicular function (5, 6). Furthermore, *in vitro*-derived sperm can serve as a platform for advanced assisted reproductive technologies, including gene editing and delivery in valuable livestock breeds (7, 8).

Recent advances in testicular tissue engineering have demonstrated that dissociated testicular cells can reorganize into testis-like structures when transplanted into immunodeficient mice (9, 10). Several studies using testicular cells from rodents or large animals have reported the formation of tubular structures and, in some cases, partial or complete spermatogenesis (11-13). In particular, xenotransplantation models provide a powerful platform for studying *in vivo* testicular morphogenesis under physiologically relevant conditions. More recently, studies have shown that growth factors such as epidermal growth factor (EGF) and glial cell line-derived neurotrophic factor (GDNF) contribute to the formation of *in vitro* testis-like structures (14, 15). Furthermore, the use of testis-derived cells from various mammals in combination with extracellular matrix components such as Matrigel has been shown to enhance tubule formation and tissue integrity by promoting three-dimensional aggregation and maintaining cell polarity (16, 17). Despite these advances, the reconstruction of functional testicular structures and complete spermatogenesis in large animal models such as pigs remains a considerable challenge due to developmental timing differences, variations in tissue composition, and limited availability of relevant materials.

Although the function of germ cells for the completion of the spermatogenic process has been

ARTICLE IN PRESS

thoroughly investigated, their role during the early stages of testicular tissue formation remains unclear. Traditionally, testis morphogenesis has been considered a somatically driven process, orchestrated primarily by Sertoli cells and peritubular myoid cells (18). However, emerging evidence suggests that germ cells may play a more active role beyond merely occupying the seminiferous cords (19). Germ cells may influence the spatial organization, vascularization, and maturation of the somatic environment itself (20). Attempts to reconstruct functional testes *in vitro* frequently encounter the challenge of germ cell depletion, where spermatogonial stem cells undergo apoptosis or fail to integrate into the developing microenvironment. This suggests that germ cells may be essential not only for spermatogenesis but also for initiating and stabilizing testis-like architecture. This raises important questions: Can testis-like structures self-organize in the absence of germ cells? If so, how do the resulting structures differ morphologically and functionally from those formed in the presence of germ cells? Addressing these questions is critical for optimizing *in vitro* testis reconstruction protocols and resolving challenges associated with testicular tissue engineering, particularly in translationally relevant large-animal models such as pigs.

In this study, we evaluated whether testis-like structures and the spermatogenic process could be induced under defined conditions, and investigated the impact of germ cell absence on testicular architecture and function under *in vitro* testis reconstitution using xenotransplantation model. These findings provide new insights into germ cell–dependent testis development and criteria for assessing functional seminiferous tubules, supporting the development of *in vitro* spermatogenesis in large animal models.

Methods

Experimental design

To systematically investigate the cellular requirements for *in vitro* testis reconstruction, we employed a xenotransplantation model using porcine testicular cells. Specifically, two experimental groups were established: (1) GF tissues, composed of both porcine spermatogonial stem cells (pSSCs) enriched germ cells and testicular somatic-enriched fraction (SEF); and (2) FO tissues, containing SEF only and lacking

ARTICLE IN PRESS

germ cells. The FO group was designed to mimic a germ cell-depleted condition, which may arise from developmental defects or environmental damage during testis-like structure formation. This comparative design enabled us to evaluate whether the presence of germ cells is critical for the formation and maturation of testis-like tissue under defined conditions. Unlike rodent models, in which primordial germ cells (PGCs) migration can be genetically manipulated (20), such interventions are technically unfeasible in large-animal species like pigs. Therefore, the use of xenotransplantation offered a practical and reproducible approach to assess testicular morphogenesis through histological, immunofluorescence, and transcriptomic analyses.

In vitro testicular cell isolation and colony formation

The animal experimental procedures used in this study were approved by the Institutional Animal Care and Use Committee of Konkuk University (KU23097). All experimental procedures involving animals were conducted in accordance with relevant guidelines and regulations. All methods are reported in accordance with the ARRIVE guidelines (https://arriveguidelines.org). Porcine testes were collected from 5-d-old, crossbred piglets (Landrace and Large White Yorkshire) sourced from Sam-Woo Livestock (Yang Pyeong, Korea). Porcine total testicular cells (pTTCs) were isolated as previously described (21). The tunica albuginea was removed, and the chopped testicular tissue was digested using five-fold volume (*v/w*) of enzyme mixture solution containing 0.01 mg/mL DNase □ (Sigma-Aldrich, MO, USA), 0.5 mg/mL collagenase □ (Gibco, CA, USA), 0.5 mg/mL hyaluronidase (Sigma-Aldrich), and 0.1 mg/mL and soy bean trypsin inhibitor (Gibco) in Dulbecco's Phosphate Buffered Saline (DPBS) at 37 □ for 15 min. After DPBS washing, second digestion (5 mg/mL collagenase IV, 0.01 mg/mL DNAse I, and 0.1 mg/mL soybean trypsin inhibitor) were conduct at 37 □ for 15 min. The digested tissue was filtered through a 40-μm nylon cell strainer (Corning, NY, USA). The collected cells were treated with an equal volume of RBC lysis buffer (Sigma-Aldrich) for 5 min to eliminate red blood cells.

Dissociated pTTCs were cultured for 1 day at 37 °C with 5% CO□ in Dulbecco's Modified Eagle Medium (DMEM) supplemented with 2% fetal bovine serum (FBS). After this attachment step, adherent SEF cells were designated feeder cells, and the suspension cell population containing pSSCs was

ARTICLE IN PRESS

collected by gentle pipetting. Fresh SEF feeder cells were harvested and cryopreserved to use subsequent injections and for continued support of pSSC colony culture.

Suspended cells were plated at 2 × 10□ cells per well on 0.1% (w/v) gelatin-coated 12-well plates and maintained at 34 °C with 5% CO□ in StemPro-34 medium (Gibco) as previously described (22), supplemented with 1% ITS (Gibco), 2 mM L-glutamine (Sigma-Aldrich), 1% non-essential amino acids (NEAA; Gibco), 1% MEM vitamin solution (Gibco), 100 U/mL penicillin–streptomycin, 1 mM sodium pyruvate (Gibco), 0.1 mM vitamin C solution (Sigma-Aldrich), 1 µg/mL lactic acid (Sigma-Aldrich), 30 ng/mL β-estradiol (Sigma-Aldrich), 60 ng/mL progesterone (Sigma-Aldrich), 0.2% bovine serum albumin (BSA; Sigma-Aldrich), 20 ng/mL mouse EGF (PeproTech, NJ, USA), 10 ng/mL basic FGF (PeproTech), 10 ng/mL GDNF (R&D Systems, MN, USA), and 10^3 U/mL LIF (Millipore, MA, USA).

To isolate pSSC colonies before overgrowth of SEF feeder cells, loosely attached colonies were gently dislodged by pipetting and transferred onto gelatin-coated 12-well plates that had been pre-seeded with 0.5 × 10□ fresh SEF feeder cells per well. Colonies were expanded for at least two passages. After colony formation, colonies were separated from SEF feeder cells by pipetting. Subsequently, a pre-plating step was performed on 0.1% gelatin-coated 100-mm dishes: cells were incubated for 1 h, twice in succession, discarding newly adherent cells each time by gentle pipetting. The non-adherent, colony-forming cells were collected and used for downstream experiments. No proliferation inhibitors (e.g., Mitomycin C) were used at any step of the cell culture procedures.

Flowcytometry

For flow cytometry analysis, colonies were first dissociated into single cells. This was achieved by incubating them in 0.25% Trypsin at 37 °C for 5 min, with gentle pipetting every minute to facilitate the process. The enzymatic reaction was subsequently neutralized using DPBS supplemented with 5% Fetal Bovine Serum (FBS). All subsequent washing and antibody steps utilized a buffer consisting of DPBS supplemented with 1% (w/v) Bovine Serum Albumin (BSA-100; Bovogen, VIC, Australia). Cells were washed in this buffer for 5 minutes and then stained with PE Mouse Anti-Human CD90 (BD Pharmingen™, catalog 561970). The primary staining was carried out for 1 hour at 4 °C. Following the

ARTICLE IN PRESS

primary incubation, cells were washed three times (5 min per wash) using the same BSA buffer. DAPI (1:1000) was utilized for nuclear counterstaining for 5 minutes, followed by three final 5 min washes. Samples were analyzed using a CytoFlex Flow Cytometry Analyzer (Beckman Coulter, CA, USA), and the resulting data was processed with CytExpert 2.6 (Beckman Coulter) software.

RNA extraction, reverse transcriptase-PCR, and quantitative-PCR

Total RNA was extracted from pSSCs and SEF cells using the RNeasy Mini Kit (Qiagen, Hilden, Germany) with an On-Column DNase Set (Qiagen). Complementary DNA (cDNA) was synthesized from 1000 ng of total RNA using the M-MLV Reverse Transcriptase Kit (Promega, Madison, WI, USA) with an oligo dT primer mix. Polymerase chain reaction (PCR) amplification of target genes was performed with 35 cycles at 95 □ for 30 s, 57 □ for 20 s, and 70 □ for 20 s. Quantitative PCR (qPCR) was performed using a 20 µL reaction mixture containing 20 ng of cDNA and 10 µL AccuPower® 2X Greenstar◉ qPCR Master Mix (Bioneer, Daejeon, Korea). The qPCR conditions were set as follows: initial enzyme activation and DNA pre-denaturation at 95 □ for 1 min, followed by 40 cycles at 95 □ for 10 s, 57 □ for 10 s, and 72 □ for 20 s. Cycle threshold (C_t) values were normalized based on the expression of the porcine β-2-microglobulin (B2M) gene. A list of primer sets is presented in Table 1.

Table 1. List of primer sets for RT-PCR and qPCR

Gene (RT-PCR)	Primer sequence (5' – 3')
B2M (166 bp)	F: TTCACACCGCTCCAGTAG R: CCAGATACATAGCAGTTCAG
UCHL1 (148 bp)	F: TCCCTTCCTATGCGGTCTAC R: ATCAGAGGCCAACATCCAAC
CD90 (512 bp)	F: ACCATTGGCATCGCTCTCTT R: GCCTTGTGGCTTCGTGTATCT
SOX9 (98 bp)	F: CATCAAGACGGAGCAGCTGA R: TGTAGTGCGGGAGGTTGAAG
GFRα1 (230 bp)	F: ATAGACTCTAGTAGCCTCAG R: AGGGACTTGTTCTTGACC

ARTICLE IN PRESS

WT1 (124 bp)	F: CTGAAGACCCACACCAGGAC R: GGTGCATGTTGTGATGACGG
Gene (q-PCR)	**Primer sequence**
B2M (166 bp)	F: TTCACACCGCTCCAGTAG R: CCAGATACATAGCAGTTCAG
CD90 (142 bp)	F: CACTCCTACCGCTCTCGAAC R: TTCTTGCTGGAGATGCTGGG
SOX9 (98 bp)	F: CATCAAGACGGAGCAGCTGA R: TGTAGTGCGGGAGGTTGAAG
WT1 (124 bp)	F: CTGAAGACCCACACCAGGAC R: GGTGCATGTTGTGATGACGG
PDGFRA (89 bp)	F: CCAGGGAGGTCAAAGAAATG R: CTTCCAAAGGGCTGAAGTTG
CD31 (133 bp)	F: CCAGAAGGACAAGGAGATCG R: TGCTGCTGACTTTGGAAATG
ACTA2 (100 bp)	F: TTTCAATGTCCCAGCCATGT R: GACACCATCTCCAGAGTCCA
STAR (158 bp)	F: GGAGGCAAGGCTCTTCTAAC R: TGACGTCCTGATCCTCTGAT
HSD3B1 (99 bp)	F: GTGTGCTCTGAGGCCCATGT R: GTTGTGTGTCAGGACGCCATT
CD9 (164 bp)	F: TTCATCTTCTGGCTCGCTGG R: AAGCCCACCACCATCATGAG
GFRα1 (230 bp)	F: ATAGACTCTAGTAGCCTCAG R: AGGGACTTGTTCTTGACC

Immunocytochemistry

Two-passaged colonies of pSSCs were cultured on glass cell culture slides (31404, SPL, Pocheon, Korea). After washing with DPBS, the cells were fixed with 4% paraformaldehyde for 10 min. Immunofluorescence (IF) buffer, containing 0.05% Triton X-100 in DPBS, was used to permeabilize the cell membrane, while 2% BSA was used to prevent nonspecific protein binding. All primary antibodies—mouse anti-human UCHL1 IgG (7863-1004; Bio-Rad, CA, USA), rabbit anti-SOX9 IgG (ab185966; Abcam, Cambridge, UK), and normal rabbit IgG (GTX35035, GeneTex, CA, USA) and mouse IgG (GTX35009; GeneTex) were treated for negative control—were diluted at 1:500 in IF buffer

ARTICLE IN PRESS

and applied to the fixed samples for overnight incubation at 4 □. Subsequently, the samples were washed twice with DPBS and incubated with Alexa Fluor 594 anti-rabbit IgG and Alexa Fluor 488 anti-mouse IgG (1:10,000, Thermo Fisher, MA, USA) secondary antibodies in IF buffer. The IF buffer was applied without primary antibodies, following the same procedure as a negative control. The samples were incubated with 1 μg/mL 4′,6-diamidino-2-phenylindole (DAPI; Thermo Fisher) for 10 min to achieve nuclear staining. Finally, samples were mounted in an aqueous mounting medium (DAKO, CA, USA), and fluorescence was observed under a confocal microscope (LSM 700; Carl Zeiss, Oberkochen, Germany).

Recipient mouse and xenograft

Four 3-week-old Balb/c immunodeficient nude male mice (DBL Co., Eumseong, Korea) were purchased and allowed a 1-week acclimatization period. Non-castration four-week-old mice were used as two recipient groups for xenotransplantation. Each mouse received four injections per group (n = 8). Mice were anesthetized with alfaxalone administered intraperitoneally at a dose of 80 mg/kg prior to cell transplantation. A total of 5×10^6 testicular cells suspended in 50 μL of StemPro-34 media and 50 μL of high-concentration Matrigel (growth factor reduced, 354263, Corning) were mixed in ice and administered into the dorsal skin using a 1-mL syringe with a 23-gauge (23-G) needle. The GF group was injected at a ratio of 1:9, consisting of 0.5×10^6 pSSC-colony cells and 4.5×10^6 fresh SEF feeder cells. All mice were maintained at 22 ± 2 °C with unrestricted access to food and water. Six months after the xenograft, immunodeficient mice were euthanized using a CO_2 chamber to collect the tissue. No specific inclusion or exclusion criteria were applied. Humane endpoints were set, including weight loss, appetite, weakness, and moribund state, but none were observed. All animals and data points were included in the analysis. The collected tissues were subjected to histological analysis.

Histology and immunohistochemistry

The reconstituted tissues were washed with DPBS and fixed overnight at 4 □ with 4% paraformaldehyde. The tissues were progressively dehydrated using a series of ethanol solutions (70–100%), immersed in

ARTICLE IN PRESS

xylene, and finally embedded in paraffin. Sections of the tissue, 5-μm thick, were cut using a rotary microtome (Thermo Fisher) and placed on glass slides. Subsequently, the sections were deparaffinized with 100% xylene and rehydrated using serial ethanol solutions (100–70%).

The sections were stained with hematoxylin and eosin (H&E) for histological analysis and observed under a microscope (Nikon, Tokyo, Japan). For the quantitative analysis of H&E-stained tissue images, a minimum of three non-overlapping fields containing clusters of tubular structures were selected and analyzed from distinct tissue sections. Qupath software (v. 0.5.1) was used to count all tubule structures to determine the total number of tubules. Among these, those characterized by the presence of cells in the germinal epithelium, a distinguishable basement membrane, and an inner array of Sertoli-like cells were classified as 'testis-like tubules'. Tubule diameter measurement was conducted by measuring the narrowest part of the tubular structure in different non-overlapping tubule-clustered sections, based on the scale bar, and the final counts of the classified tubules were recorded for subsequent statistical analysis.

Additionally, antigen retrieval was performed by boiling the sections in 10 mM sodium citrate buffer (pH 6.0) for 15 min for immunohistochemical analysis. The primary antibodies (Table 2) and same dilution of normal rabbit and mouse IgG for negative control were diluted in IF buffer and applied to the sections overnight at 4 □. Sections were then rinsed with DPBS and incubated with secondary antibodies (diluted 1:1000: Alexa 488 anti-mouse (A32723), Alexa 568 anti-mouse (A11004), Alexa 594 anti-rabbit (A11012), and Alexa 488 anti-rabbit (A11008) for 1 h at room temperature (24-26 □). Subsequently, 1 μg/mL of DAPI was applied to the sections for 10 min to stain the nuclei, followed by washing with DPBS. The sections were then mounted using an aqueous mounting medium (DAKO) and examined under an LSM 700 confocal microscope. For quantitative analysis of immunohistochemical analysis, images were captured by tile capture method for merging whole section and counted using Qupath software.

Table 2. List of primary antibodies for immunofluorescence staining

Antibody	Catalog number	Manufacturer	Dilution

ARTICLE IN PRESS

UCHL1 (PGP9.5)	7863-1004	Bio-Rad	1:200
SOX9	AB185966	Abcam	1:200
DDX4 (VASA)	SC-517247	Santa Cruz	1:200
ACR	SC-51504	Santa Cruz	1:100
PRM2	14500-1-AP	Proteintech	1:100
wAMH (MIS)	SC-166752	Santa Cruz	1:100
WT1	MA5-32215	Invitrogen	1:100
AR	PA1-110	Invitrogen	1:100
DMRT1	PA5-79160	Invitrogen	1:100
NR5A1	PA5-41967	Invitrogen	1:100
ESR1 (ERα)	SC-787	Santa Cruz	1:100
FOXL2	PA1-802	Invitrogen	1:100

238

239 **Tissue RNA isolation, library preparation, and sequencing**

240 Total RNA was isolated from 5-d-old (5D) testes (only displayed in additional file 3), GF and FO tissues
241 using TRIzol reagent (Invitrogen, USA). RNA quality was assessed using an Agilent 4200 TapeStation
242 System (Agilent Technologies, USA), and RNA quantification was performed using a Qubit (Thermo
243 Fisher). A library was constructed using the QuantSeq 3' mRNA-Seq Library Prep Kit (Lexogen,
244 Austria) according to the manufacturer's instructions for control and test RNAs. In brief, total RNA
245 from each sample was prepared. An oligo-dT primer containing an Illumina-compatible sequence at its
246 5′ end was hybridized to the RNA, and reverse transcription was performed. After degradation of the
247 RNA template, second strand synthesis was initiated by a random primer containing an Illumina
248 compatible linker sequence at its 5′ end. The double-stranded library was purified using magnetic beads
249 to remove all reaction components. The library was then amplified to add complete adapter sequences
250 required for cluster generation, and the final library was purified from the PCR components. High-
251 throughput single-end 75 sequencing was performed using a NextSeq 550 (Illumina, USA).

252

253 **Data analysis**

ARTICLE IN PRESS

Quality control of the raw sequencing data was performed using Fast QC (23). QuantSeq 3' mRNA-Seq reads were aligned using the Spliced Transcripts Alignment to a Reference (STAR) program (24). STAR indices were generated from either the genome assembly sequence or representative transcript sequences for alignment to the genome and transcriptome. The alignment file was used to assemble transcripts, estimate their abundance, and detect differential gene expressions (DEGs).

DEGs were determined based on counts from unique and multiple alignments using coverage from HTSeq counts (25). The Read Count (RC) data were processed based on the Trimmed Mean of M-values + Counts per million (TMM + CPM) normalization using the EdgeR method and DEseq2 (v1.42.0) (26). Gene classification was based on searches performed using the Database for Annotation, Visualization, and Integrated Discovery (DAVID; http://david.abcc.ncifcrf.gov/) and Medline databases (http://www.ncbi.nlm.nih.gov/). Data mining and graphic visualization were performed using ExDEGA (Ebiogen, Seoul, Korea) and Rstudio (v4.3.1). The heatmap and Gene Ontology Biological Process (GOBP) plot were constructed using ComplexHeatmp (v2.16.0) and ClusterProfiler (v4.8.2).

Statistical analysis

GraphPad Prism was used for data analysis. All data are presented as the mean ± standard errors of the mean (SEM). A *t*-test was used for statistical testing between the control and the sample. The null hypothesis was rejected, when the probability was < 0.05.

Results

Characterization of pSSCs and SEF feeder cells used for xenograft

Immunocytochemistry (ICC) was performed to characterize pSSCs and SEF feeder cells before injection. The pSSC colonies were positively stained for UCHL1 and DDX4, while SOX9 expression was observed in SEF feeder cells but not in the colonies (Fig. 1a). After isolating pSSC colonies from SEF feeder cells, RT-PCR and qPCR were performed to verify their characteristics and separation efficiency. *UCHL1* was observed in both pSSCs and SEF feeder cells. The gene expression of the SSC marker *CD90* and *GFRα1* were not identified in SEF feeder cells but were observed in pSSCs (Fig. 1b).

ARTICLE IN PRESS

However, the expressions of *WT1* and *SOX9*, which are markers of Sertoli cells, were observed mainly in SEF feeder cells, while lower expression was identified in pSSCs (Fig. 1b). In addition, qPCR data revealed a significant increase in *CD90* ($p < 0.001$) expression in pSSCs, whereas notable differences in *WT1* ($p < 0.001$) and *SOX9* ($p < 0.001$) expression were observed in SEF feeder cells, with fold changes of 3.7 and 6.4, respectively (Fig. 1c). To validate the characteristics of SEF feeder cells and pSSC colonies, gene expression relative to pTTC was assessed by RT- and qPCR. In SEF feeder cells, bands of *PDGFRA* (stromal cell marker), *CD31* (PECAM1; vascular endothelial cell marker), *ACTA2* (α-SMA; peritubular myoid cell marker), *STAR* (Leydig cell marker), *HSD3B1* (Leydig cell marker), *SOX90*, and *WT1* were observed, but *PDGFRA, CD31, STAR, HSD3B1* were relatively lower than pTTCs (Fig. 1d). In qPCR, expression of genes representing testicular somatic cell components showed the following patterns: *PDGFRA*, no significant difference; *CD31*, significantly decreased ($p < 0.05$); *ACTA2*, no significant difference; Leydig cell–related genes *STAR* and *HSD3B1*, significantly decreased ($p < 0.001$); *SOX9*, no significant difference; *WT1*, significantly decreased ($p < 0.05$; Fig. 1e). In pSSC colonies, *UCHL1* ($p < 0.001$), *CD90* ($p < 0.001$), *CD9* ($p < 0.001$), and *GFRA1* ($p < 0.05$) were significantly increased relative to pTTC (Fig. 1f). Additionally, verification of the absence of differentiation during *in vitro* culture of germ cells is presented in additional file 1d. Flowcytometry further showed that the CD90-positive population in pSSC colonies was approximately 75%, significantly higher than in pTTC (Fig. 1g), gating strategy is presented in additional file 2. These cells were subsequently injected into the dorsal skin of 4-week-old BALB/c nude mice.

Formation and histological characterization of xenograft tissues

Six months after testicular cell transplantation into immunodeficient mice, reconstructed tissues were extracted from the dorsal skin. Recovery rates of GF and FO tissues were listed in Table 3. GF tissues showed the development of blood vessels (red arrows) between the mouse skin and the reconstructed tissues (Fig. 2a and b). Although FO tissues also exhibited development of blood vessels, it was less extensive (Fig. 2a and b). Particularly, the GF tissues displayed a three-dimensional spherical morphology, whereas the FO tissues had a flattened and oval configuration (Fig. 2a). Furthermore, GF

ARTICLE IN PRESS

tissues formed a single cohesive structure (white arrows) following cell injection, whereas FO tissues formed two separate structures (yellow arrows) after each injection (Fig. 2a). Additionally, blood vessels persisted on the surface of GF tissues following isolation and washing but were fewer on FO tissues (Fig. 2b).

H&E-stained GF tissues revealed prepubertal and mature testicular organization, featuring seminiferous tubule-like structures of various sizes. These tubules were clearly distinguishable from the surrounding interstitial area (Fig. 2c and d). A group of these seminiferous tubules, along with their interstitial areas, was demarcated by tunica albuginea-like tissue (TAL; Fig. 2c). In addition, Sertoli cells were aligned along the basement membrane, similar to the typical testis structure, as shown at high magnification (Fig. 2c and d). Among the different tubule sizes, the most dilated tubules exhibited a mature-like structure, including a well-developed lumen within the germinal epithelium. These tubules consisted of a complex germinal epithelium and a thick basement membrane (Fig. 2d).

FO tissues showed a more heterogeneous structure than GF tissues, with simple tubular development (Fig. 2e-g). The central region of the FO tissues exhibited other types of tissues in addition to the tubular shape (Fig. 2e-g). Moreover, none of the circular structures formed a pattern of normal seminiferous tubules or interstitial areas (Fig. 2e-g). The outer lining of the simple tubules was composed of cells that lacked the basement membrane typically found in seminiferous tubules. In addition, the inner mass of these tubules appeared to be separated from the outer lining (Fig. 2e-g).

At 100× magnification, counts of tubule clusters indicated that GF tissues contained more total tubules than FO tissues ($p < 0.001$; Fig. 2h). Both small (<100 μm diameter) and large (≥100 μm) tubular structures were also significantly more frequent in GF ($p < 0.01$). Although the absolute number of testis-like tubules was higher in GF, the proportion of tubules with empty lumina did not differ between groups (Fig. 2i). Mature-like tubules with well-defined lumens were composed of about 24% (Fig. 2i).

Table 3. Recovery rate of collected from xenotransplantation.

Group	Graft number (n)	Recovered tissue (N)	Recovery rate (N/n×100%)
GF tissue	8	9	112.5%

ARTICLE IN PRESS

FO tissue	8	14	175%

333

334

335 **Comparison between GF tissues and normal testis**

336 A broader interstitial area containing interstitial cells was observed in 5D testes. Here, Sertoli cells and
337 germ cells were attached to the basement membrane of the tubules (Fig. 3a). Notably, spermatogonia
338 were located on both the basement membrane and germinal epithelium (Fig. 3a). Similar to the 5D
339 testes, a wide range of interstitial areas with interstitial cells was also observed in GF tissues. Sertoli
340 cells along with spermatogonia were identified within the basement membrane, with spermatogonia
341 further located in the germinal epithelium (Fig. 3b). The expanded tubules and interstitial area were
342 relatively reduced, and fully integrated spermatogonia located between Sertoli cells were identified on
343 the basement membrane in both the 90-d-old (90D) testes and GF tissues (Fig. 3c and d). Some GF
344 tissue sections exhibited mature seminiferous tubule morphology. Compared with fully mature 150-d-
345 old (150D) testes, GF tissue showed an increase in the cell population within the germinal epithelium;
346 spermatogonia were positioned along the basement membrane (Fig. 3e and f). Moreover, both
347 differentiating germ cells and round spermatids were observed within the germinal epithelium, while
348 elongated spermatids were detected at the boundary between the germinal epithelium and lumen in both
349 the 150D testis and GF tissue (Fig. 3e and f).

350 UCHL1-and SOX9 protein expression was determined in pSSCs and Sertoli cells, respectively, to
351 characterize the cellular composition of the normal testis and GF tissue. The PGP 9.5-positive
352 spermatogonia were primarily localized to both the basement membrane (white arrows) and seminal
353 cords (yellow arrows) of 5D testes and GF tissues (Fig. 3g), whereas SOX9-positive Sertoli cells were
354 placed their basement membranes (Fig. 3g). In contrast to the 5D testes, the interstitial area of the GF
355 tissue also contained SOX9-positive cells (blue arrows; Fig. 3e). When comparing 90D testes with GF
356 tissues, PGP 9.5-positive spermatogonia were detected in both samples, mainly located between SOX9-
357 positive Sertoli cells on the basement membrane (Fig. 3h). The interstitial areas of the GF tissues also
358 contained SOX9-positive cells (blue arrow; Fig. 3g).

ARTICLE IN PRESS

Staining for UCHL1, DDX4, and ACR was performed to confirm spermatogenesis in spermatogonia within GF tissues, compared with 150-d-old normal testis (150D). UCHL1 expression was noted in germ cells on the basement membrane. DDX4, a marker of differentiating spermatocytes, was detected in cells of the germinal epithelium of tubules in both GF and 150D testis tissue (Fig. 3i). Subsequently, ACR-expressing cells were identified among the DDX4-positive cells in both 150D and GF tubules (Fig. 3j). Protamine expression was also observed in some elongated spermatids expressing ACR (Fig. 3m). Their ACR expression patterns distinctly determined the Golgi, cap, and acrosome phases of spermatocyte development into elongated spermatids (Fig. 3l). When positive tubules were counted for quantitative analysis, the proportion of tubules expressing UCHL1 was significantly the highest at 45% ($p < 0.05$), followed by tubules expressing VASA at 27% and tubules expressing ACR at 14% (Fig. 3m).

Examination of characteristics of Sertoli cells in GF and FO tissues

Immunostaining for AMH, WT1, AR, DMRT1, and NR5A1 (SF1) was performed to assess the characteristics of Sertoli cells in the GF and FO tissues. FOXL2 and ESR1 (ERα) were additionally examined to evaluate potential feminization features in the FO group. The expression of AMH, a prepubertal Sertoli cell marker, was detected in the inner region of GF and FO tissues (Fig. 4a). The germinal epithelium of GF tubules was filled with AMH-positive cytoplasm of Sertoli cells (Fig. 4a). Notably, AMH staining was also observed in the inner regions of the tubules in FO tissues (Fig. 4a'). SOX9 expression was detected in the basement membrane of GF tissues (Fig. 4a); however, FO tissues showed limited expression in the inner region but not the peripheral region of the tubules (Fig. 4a'). Furthermore, relatively weak expressions of both AMH and SOX9 were observed in the borderline of the FO tubules (Fig. 4a').

Subsequently, WT1, a whole-stage marker of Sertoli cells, was observed in the basement membrane of GF tissues, and its expression was determined in the cells expressing SOX9 (Fig. 4b). Moreover, WT1 expression was detected not only in the inner region of the tubules but also in outer cell lining of the FO tubules (white arrows; Fig. 4b'). AR, a marker of mature Sertoli cells, was clearly observed in

ARTICLE IN PRESS

the basement membrane and germinal epithelium in GF tissues (Fig. 4c). However, AR-positive Sertoli cells were absent in FO tissues (Fig. 4c'). DMRT1 was predominantly expressed along the basement membrane of GF tubules, whereas only weak staining was observed in the inner regions of FO tubules (Fig. 4d'). NR5A1, also known as steroidogenic factor 1 (SF1), exhibited a similar expression pattern to AR in GF tubules (Fig. 4e). In FO tissues, NR5A1 was more strongly expressed in the inner region of the tubules compared to the peripheral areas (Fig. 4e).

To investigate the expression of feminization proteins expressed when Sertoli cell characteristics are lost, staining for FOXL2 and ESR1 was performed. In GF, ESR1 was observed to be expressed in some interstitial areas (Fig. 4g), whereas in FO tissue, ESR1 expression was relatively more abundant on the outer side of the tubule (Fig. 4f'). Granulosa cell marker was hardly expressed in GF (Fig. 4g), but FOXL2 was expressed in cells forming the outer line of the tubule in FO (Fig. 4g').

DEG profiling between GF and FO tissues

DEG profiling of 5D testis, GF and FO tissues are presented in Additional file 3, and in the main text only GF and FO tissues were compared. The heatmap of significant genes related to spermatogenesis was divided into three clusters based on the morphology of the testes at various developmental stages in the GF tissues to further investigate Gene Ontology Biological Processes (Fig. 5a). Cluster 1 included *TDRD5*, *TDRD6*, *BAG6*, *STRBP,* and *ZBTB16*, which are involved in spermatogonial development. Cluster 2 included genes, such as *ZCWPW1*, *TNP1*, *PRM1*, *RSPH1*, *CFAP69,* and *CFAP43*, which are essential genes for spermatozoa. Cluster 3 included *JAM3*, *SLC19A2*, and *EPC1*, involved with gamete generation. Based on the hallmark Gene Set Enrichment Analysis (GSEA), the overall gene expression enrichment score (ES) for GF tissues revealed significant GOBPs related to germ cell differentiation. The normalized enrichment score (NES) represents the score of genes that were particularly enriched for overall gene expression. GSEA results indicated that gene sets related to cell cycle regulation, such as "E2F targets" and the "G2M checkpoint," along with "spermatogenesis," were highly enriched in GF tissues (Fig. 5d). Specifically, "spermatogenesis" exhibited a NES of 2.76, "E2F targets" showed an NES of 2.01, and the "G2M checkpoint" displayed an NES of 1.89 (Fig. 5b).

ARTICLE IN PRESS

In significantly upregulated genes in the GF tissue, various terms related to spermatogenesis-associated biological processes were highlighted. Notably, the upregulated genes were associated with key testicular functions, including "reproduction" and "gamete generation" (Fig. 6c). The Gene-Concept Network (CNET) plot illustrates the association between specific GOBPs. A CNET plot analysis was performed for genes related to "reproduction," "gamete generation," "spermatogenesis," "germ cell development," and "meiosis I." Expression of *NR5A1*, *AMH*, *AR,* and *DMRT1* was detected in Sertoli cells. Among the germline cell-associated genes, key genes were involved in the progression of spermatogenesis, including *MAEL*, *RARA*, *PIWIL1*, *PRM1*, *PRM2*, *TNP*, *DAZAP1*, *SPATA6*, and *HORMAD1*. Moreover, genes related to fertilization capacity, such as *ACR*, *ACRBP*, *MAEL*, *ACTL9*, and *YBX3*, were also expressed in GF tissues (Fig. 6d).

Focusing on gene expression in FO tissues, a heat map was constructed with significant genes involved in coagulation. Cluster 1, involved in cell adhesion and extracellular matrix (ECM) remodeling, was predominantly present in FO tissue. The expressions of *TIMP1*, *TIMP3*, *MMP2*, *FN1*, *KLF7,* and *CAPN2* were specifically examined. Moreover, the expression of inflammatory genes, such as *C3*, *C1R*, and *CFI,* was observed (Fig. 5e). These results were further validated using the enrichment scores of FO tissues in the GSEA. Gene sets related to "coagulation," "epithelial-mesenchymal transition," and "apoptosis" displayed high enrichment scores of -2.29, -2.24, and -2.02, respectively (Fig. 5f).

The GOBP dot plot of FO tissues showed gene expression patterns related to "tissue development" and "tube morphogenesis" but not testicular development. Instead, GOBP of the FO tissue represented circulatory and vasculature-related processes. Additionally, GOBPs related to "locomotion" and "epithelial-mesenchymal transition" were observed (Fig. 6g). The CNET plot of FO tissues illustrated genes involving "tissue development," "epithelium development," "tube development," and "mesenchyme development." Briefly, BMP-WNT signaling genes, such as *BMP2*, *BMP4,* and *WNT5A,* were expressed. JAK-STAT signaling genes, such as *LIF*, *JAK2*, *STAT1,* and *STAT6*, were also displayed. Additionally, genes involved in pre-Sertoli and gonadal development, including *NR2F2*, *WT1*, *FGF18*, *ACVR1*, *ESR1,* and *TGFBR,* and tubule formation-related genes, including *GJA5*, *ITGAV*, *AGTR1*, *VEGFA,* and *CD109*, were expressed (Fig. 6h).

ARTICLE IN PRESS

Discussion

A previous study reported that a high germ cell proportion (3–25%) in Matrigel promoted seminiferous tubule formation, with no added benefit at higher ratios (> 25%) (14). Based on this, we used a germ cell proportion of 10% of total cells, which lies within the optimal range. In this study, pSSC-enriched colony cells showed increased mRNA levels of UCHL1, CD90, CD9, and GFRA1 relative to pTTCs, and flowcytometry confirmed a high frequency of CD90-positive cells, indicating enrichment of pSSC features. In line with previous reports, colony-formed pSSCs were enriched to obtain cells with high self-renewal capacity and stemness, as indicated by elevated expression of UCHL1, PLZF, OCT4, NANOG, and GFRA1 (27, 28). Compared with freshly isolated germ cells, colony-forming pSSCs engage more robustly with testicular somatic cells and constitute a more homogeneous population, which may improve the reproducibility and efficiency of testicular tissue reconstruction. Characterization of SEF feeder cells showed no CD90 and CD9 expression, indicating that germ cells were not included in this fraction. Testicular somatic cells have been described as comprising Sertoli cells, peritubular myoid cells, Leydig cells, and stromal/interstitial cells (29). To define these cellular properties, expressions of *PDGFRA*, *CD31*, *ACTA2*, *STAR*, *HSD3B1*, *SOX9*, and *WT1* were detected in the SEF feeder cells. Because adherent cells were selectively collected during the attachment step, relative enrichment of stromal cells, vascular endothelial cells, and Sertoli cells and decrease of Leydig cells were observed. Accordingly, transplantation in this study was performed under somatic-cell conditions characterized by relatively fewer Leydig and endothelial cells, with relative enrichment of stromal cells, peritubular myoid cells, and Sertoli cells. A modified StemPro34 medium, optimized for the maintenance of porcine spermatogonial stem cells, was used as the basal medium to enhance germ cell survival (16, 27). This differs from earlier studies that employed DMEM or DMEM/F12 as the basal medium (9, 10, 14, 17). Further, the medium was supplemented with EGF, FGF2, LIF, and GDNF to support the survival of spermatogonia and facilitate early aggregation. Notably, Recent studies have shown that these growth factors, when combined, facilitate the initiation of testis cord formation during the early stages of reconstruction (15, 30).

ARTICLE IN PRESS

ARTICLE IN PRESS

The reconstructed GF tissues exhibited active vascularization and formed large, spherical grafts with well-organized tubule-like structures, indicating that germ cells promote testicular morphogenesis. This aligns with earlier findings that immature testicular cell grafts promote vascular ingrowth (31). In contrast, FO tissues showed limited vascularization and developed into fragmented, small grafts (14 grafts from 8 injections) composed of simple or pseudo-tubules. DEG analysis revealed strong enrichment of coagulation pathways, which showed the highest NES among FO-associated signatures and are typically linked to tissue injury, inflammatory repair responses, and progression toward fibrosis. FO tissues also exhibited selective upregulation of ECM-related genes compared with 5-d-old testes (Additional file 3D). This likely reflects the high baseline angiogenic activity of neonatal testes, where vascular- and angiogenesis-related pathways are already maximally active, making ECM remodeling the predominant detectable change. Morphologically, FO grafts resembled Sertoli Cell-Only Syndrome (SCOS) testes (32), and germ cell–depleted mouse testes (33), as their transcriptome profiles revealed upregulation of inflammation- and apoptosis-related genes (34). Collectively, these results underscore the indispensable role of germ cells to somatic coordination required for proper angiogenesis and testicular morphogenesis.

Although several studies have described the morphological reconstruction and partial spermatogenesis following dorsal skin transplantation of testicular cells (9, 12, 14), evidence for sequential spermatogenesis remains limited. In this study, GF tissues displayed organized seminiferous tubules with appropriate positioning of spermatogonia, and germ cells spanning spermatocytes to spermatids were identified. The spatial distribution of germ and Sertoli cells resembled that of intact porcine testes. Strong DDX4 expression supported ongoing spermatogenic progression from undifferentiated spermatogonia to mature spermatids (35, 36). Detection of ACR, a marker of spermiogenesis, further indicated the presence of spermatids undergoing Golgi, cap, and acrosome phases (37). Furthermore, PRM2, a key component involved in the final stage of spermiogenesis (38), were detected in GF tissue. These findings validate the functional reconstruction of the xenografted tissue and highlight the essential role of pSSCs in establishing a competent testicular microenvironment.

To investigate the formation of a functional germ cell-Sertoli cell niche, Sertoli cell characterization

ARTICLE IN PRESS

was conducted between GF and FO tissues. FO tissues exhibited pronounced defects in Sertoli cell arrangement, polarity, and function, highlighting the challenges of maintaining testicular architecture. Although WT1, an early gonadal marker known to support NR5A1 expression for testis development (39-41), was still expressed in both GF and FO tissues, other key regulators of Sertoli cell identity such as SOX9, AR, DMRT1, and NR5A1 (42-45) showed abnormal localization or diminished expression in FO tissues. This is consistent with earlier reports of disorder of sex development (DSD) showing that loss of germ cell-Sertoli cell interactions during early testis development results in disorganized tubule formation and reduced Sertoli cell specialization (46, 47). Furthermore, this observation is consistent with germ cell-depleted mouse models, in which loss of germ cells alters Sertoli cell transcriptional programs and produces an abnormal, non-cycling Sertoli state distinct from that in germ cell-sufficient testes (33, 48, 49). Specifically, Similar to germ cell–deficient mouse models in which PGC specification is impaired Blimp1/Prdm1 or Prdm14 mutants (50, 51), the FO xenografts in this study represent a germ-cell–free testicular environment from the outset. The most notable results were FOXL2 and ESR1 in FO tissues, Ectopic FOXL2 expression in FO tissues further supports a shift toward a feminized somatic fate, as FOXL2 upregulation in XY gonads or postnatal testes is a hallmark of male-to-female reprogramming following disruption of DMRT1 or SOX9 function (52, 53). To our knowledge, this appears to be the first report of FOXL2 expression in the absence of germ cells in porcine species. In parallel, ESR1 expression in FO tissues suggests increased sensitivity to estrogen signaling, which has been shown to be mediated by nuclear ESR1 in Sertoli cells and to modulate Sertoli transcriptional activity (54, 55).

Bulk RNA-seq analysis corroborated the morphological findings. GF tissues showed strong enrichment of cell cycle and spermatogenesis-related pathways, and stage-specific germ cell signatures were evident in the heatmap. CNET analysis confirmed high expression of mature spermatid genes (ACR, ACRBP, PRM1, PRM2), consistent with active spermatogenesis (56). PCA revealed dispersed GF samples and tightly clustered FO samples, indicating developmental progression versus uniform arrest (Additional file 3a). Correlation analysis further positioned 5D testes between GF and FO tissues (Additional file 3c). Notably, GF1 and GF4 of RNA samples, which displayed less advanced tubule

ARTICLE IN PRESS

morphology, also occupied intermediate transcriptomic positions, suggesting partial rather than complete maturation. These results indicate that reconstruction of functional testis-like tissues depends not solely on transplantation duration, but on the early establishment of an appropriate germ cell-Sertoli cell niche formation.

GOBP analysis revealed that GF tissues were significantly enriched for Sertoli cell-specific biological processes, including those involving *NR5A1*, *AMH*, *AR*, and *DMRT1* This enrichment reflects the successful activation of male developmental pathways and the establishment of a well-organized testicular architecture. In contrast, FO tissues lacked such testis-related enrichment and instead showed upregulation of genes involved in early developmental pathways. Notably, genes such as *BMP2*, *BMP4*, *WNT5A*, *TGFBR3*, *ACVR1*, *FOXL2* and *ACVR2B*, which are typically repressed during male gonad differentiation (57, 58), were prominently expressed in FO tissues, indicating a failure to suppress developmental pathways incompatible with testis formation. This dysregulation is closely linked to the absence of germ cells, which are known to promote SOX9 activation via FGF signaling, suppression of feminization pathways through DMRT1, and inhibition of TGFβ/activin signaling (55, 59). These molecular features reinforce the conserved role of germ cells in orchestrating Sertoli cell maturation and testis formation across species (20), highlighting their indispensable function in establishing a male-specific gonadal environment. Collectively, these observations provide a critical molecular criterion for distinguishing true testis-like structures from simple or pseudo-tubular formations in *in vitro* testis generation.

Collectively, preserving and incorporating spermatogonia into xenograft models will therefore be essential for producing functional, transplantable testis-like structures and for enabling scale-up in future applications. In this context, we expect that our findings will provide useful insights for overcoming current challenges in testis reconstruction for *in vitro* spermatogenesis, including incomplete seminiferous tubule formation and germ cell loss. This was achieved by combining pre-conditioned pSSCs with an optimized medium containing high-concentration Matrigel. These results have important implications for livestock biotechnology, particularly for advancing in vitro spermatogenesis techniques that support reproductive efficiency, preservation of superior genetic traits, and the generation of

ARTICLE IN PRESS

transgenic large animals for agricultural and biomedical purposes.

Nevertheless, the partial success in testis morphogenesis and spermatid development observed in this study, several limitations remain. Although our data are statistically significant, the relatively small sample size necessitates cautious interpretation when extrapolating the results. Leydig cell immunostaining was attempted; however, the signals were inconsistent, possibly due to antibody compatibility with xenografted porcine tissue. Detailed characterization of spermatid subtypes was not conducted, consistent control over developmental stages was not achieved, and the fertilizing ability of the sperm, as well as their capacity to support embryo development, has yet to be confirmed. Further studies are also needed to clarify how germ cell deficiency contributes to gonadal dysgenesis, which will be crucial for optimizing germ cell-somatic cell interactions in future testis reconstruction platforms.

Conclusion

During the xenotransplantation experiments, the combination of porcine testicular cells containing colony-forming pSSCs with modified StemPro-34 (+EGF, FGF, GDNF, LIF) and concentrated Matrigel resulted in the successful assembly of tissue that closely resembled the native porcine testis. Germ cells played an indispensable and central role in influencing the alignment of somatic cells and the formation of seminiferous tubules. Without the pSSCs, the grafts consistently failed to organize like SOCS or DSD models, clearly demonstrating the fundamental dependence of organized *in vitro* testis formation and development on germ cell input. The xenograft model successfully reproduced key structural and cellular patterns observed *in vivo*, thereby providing clear criteria to distinguish true testis-like structures from pseudo-tubules, making it a practical framework for studies in livestock reproduction. This work establishes a practical framework for studies in livestock reproduction and could be used to address challenges such as fertility recovery, preservation of superior genetic lines, and the generation of genetically modified animals.

List of abbreviations

ACR: acrosin

ARTICLE IN PRESS

ACRBP: acrosin binding protein

ACTL9: actin-like 9

ACVR1: activin A receptor, type I

AGTR1: angiotensin II receptor type 1

AMH: anti-Müllerian hormone

AR: androgen receptor

BAG6: BAG Cochaperone 6

BMP: bone morphogenetic protein

C1R: complement component 1, r subcomponent

C3: Complement component 3

CAPN2: Calpain-2 catalytic subunit

CD109: cluster of differentiation 109

CD90: cluster of differentiation 90

CFAP: cilia and flagella associated protein

CFI: complement factor I

DAZAP1: DAZ-associated protein 1

DMRT1: doublesex and mab-3 related transcription factor 1

EGF: epidermal growth factor

ESR: estrogen receptor, ERα

FGF: fibroblast growth factor

FN1: fibronectin 1

GDNF: glial cell line-derived neurotrophic factor.

GFRα1: GDNF family receptor alpha 1

GJA5: gap junction protein alpha 5

GOBP: gene ontology biological process

ITGAV: integrin subunit alpha V

JAK: Janus kinase

ARTICLE IN PRESS

ARTICLE IN PRESS

KLF7: Kruppel-like factor 7

LIF: leukemia inhibitory factor

MAEL: maelstrom spermatogenic transposon silencer

MMP: matrix metalloproteinase

NR2F2: nuclear receptor subfamily 2, group F, member 2

NR5A1: nuclear receptor subfamily 5, group A, member 1

UCHL1: Ubiquitin Carboxyl-Terminal Hydrolase L1

PIWIL1: Piwi-like RNA-mediated gene silencing 1

PRM: protamine

RARA: retinoic acid receptor alpha

RSPH1: radial spoke head component 1

SOX9: SRY-box transcription factor 9

SPATA6: spermatogenesis associated 6

SRY: sex-determining region Y

STAT: signal transducer and activator of transcription

STRBP: spermatid perinuclear RNA binding protein

TDRD: Tudor domain containing

TGFBR3: transforming growth factor beta receptor 3

TIMP: tissue inhibitor of metalloproteinase

TNP: transition protein

DDX4 (VASA): DEAD-box helicase 4; a conserved germ cell-specific RNA helicase

VEGFA: vascular endothelial growth factor

WNT: wingless-related integration site

WNT5A: wingless-type MMTV integration site family, member 5A

WT1: Wilms' tumor gene 1

YBX3: Y-box binding protein 3

ZBTB16: zinc finger and BTB domain-containing protein 16

ARTICLE IN PRESS

ARTICLE IN PRESS

ZCWPW1: zinc finger CW-type and PWWP domain containing 1

Declarations

Ethics approval and consent to participate

This study followed the standard operating guidelines for experimental animals of the Korean Ministry of Food and Drug Safety and Animal and Plant Quarantine Agency. The project, titled "Evaluation of the function of CD14 in the niche homing mechanism of porcine spermatogonia," was approved by the Institutional Animal Care and Use Committee (IACUC) of Konkuk University with approval number KU23097. No human cells or samples were involved in this study.

Consent for publication

Not applicable.

Data availability

The raw sequencing data generated in this study are available in the NCBI Sequence Read Archive (SRA) under accession number PRJNA1197989.

ARTICLE IN PRESS

Competing interests

The authors declare no competing interests.

Funding

This study was supported by grants from the National Research Foundation of Korea (NRF)-2022R1A2C1004503.

Author contributions

ARTICLE IN PRESS

M.G.H. conducted most of the experiments and analyzed the data. **Y.J.** and **H.M.** performed primary cell isolation and xenografts. **D.K.** contributed to the examination of porcine total cell characteristics. **J.T.D., K.H.,** and **Y.S.** interpreted the data. **M.G.H.** and **H.S.** prepared the manuscript.

Acknowledgements

The authors thank the Sam-Woo livestock for providing porcine testis samples and Editage (www.editage.co.kr) for editing and reviewing this manuscript for English language.

References

1. Knox RV. Swine fertility in a changing climate. Animal Reproduction Science. 2024;269:107537.
2. Sato T, Katagiri K, Gohbara A, Inoue K, Ogonuki N, Ogura A, et al. In vitro production of functional sperm in cultured neonatal mouse testes. Nature. 2011;471(7339):504–7.
3. Savvulidi F, Ptacek M, Savvulidi Vargova K, Stadnik L. Manipulation of spermatogonial stem cells in livestock species. J Anim Sci Biotechnol. 2019;10:46.
4. Nakami W, Kipyegon AN, Nguhiu-Mwangi J, Tiambo C, Kemp S. Culture of spermatogonial stem cells and use of surrogate sires as a breeding technology to propagate superior genetics in livestock production: A systematic review. Vet World. 2021;14(12):3235–48.
5. Zhao X, Wan W, Zhang X, Wu Z, Yang H. Spermatogonial Stem Cell Transplantation in Large Animals. Animals (Basel). 2021;11(4).
6. Kanatsu-Shinohara M, Ogonuki N, Inoue K, Miki H, Ogura A, Toyokuni S, et al. Long-term proliferation in culture and germline transmission of mouse male germline stem cells. Biol Reprod. 2003;69(2):612–6.
7. Sun YZ, Liu ST, Li XM, Zou K. Progress in in vitro culture and gene editing of porcine spermatogonial stem cells. Zool Res. 2019;40(5):343–8.
8. Bishop TF, Van Eenennaam AL. Genome editing approaches to augment livestock breeding programs. J Exp Biol. 2020;223(Pt Suppl 1).
9. Honaramooz A, Megee SO, Rathi R, Dobrinski I. Building a testis: formation of functional testis tissue after transplantation of isolated porcine (Sus scrofa) testis cells. Biol Reprod. 2007;76(1):43–7.
10. Watanabe T, Hayashi H, Kita K, Kubota Y, Ogawa T. Ectopic porcine spermatogenesis in murine subcutis: tissue grafting versus cell-injection methods. Asian J Androl. 2009;11(3):317–23.
11. Gassei K, Ehmcke J, Wood MA, Walker WH, Schlatt S. Immature rat seminiferous tubules reconstructed in vitro express markers of Sertoli cell maturation after xenografting into nude mouse hosts. Mol Hum Reprod. 2010;16(2):97–110.
12. Zeng W, Alpaugh W, Stefanovski D, Schlingmann K, Dobrinski I, Turner RM. Xenografting of isolated equine (Equus caballus) testis cells results in de novo morphogenesis of seminiferous tubules but not spermatogenesis. Andrology. 2017;5(2):336–46.
13. Shetty G, Mitchell JM, Lam TNA, Wu Z, Zhang J, Hill L, et al. Donor spermatogenesis in de novo formed seminiferous tubules from transplanted testicular cells in rhesus monkey testis. Hum Reprod. 2018;33(12):2249–55.
14. Dores C, Dobrinski I. De novo morphogenesis of testis tissue: an improved bioassay to investigate the role of VEGF165 during testis formation. Reproduction.

ARTICLE IN PRESS

2014;148(1):109–17.
15. Awang-Junaidi AH, Fayaz MA, Goldstein S, Honaramooz A. Brief exposure of neonatal testis cells to EGF or GDNF alters the regenerated tissue. Reprod Fertil. 2022;3(1):39–56.
16. Lee KH, Lee WY, Kim DH, Lee SH, Do JT, Park C, et al. Vitrified canine testicular cells allow the formation of spermatogonial stem cells and seminiferous tubules following their xenotransplantation into nude mice. Sci Rep. 2016;6:21919.
17. Zhang D, Jin W, Cui Y, He Z. Establishment and Characterization of Testis Organoids with Proliferation and Differentiation of Spermatogonial Stem Cells into Spermatocytes and Spermatids. Cells. 2024;13(19).
18. O'Donnell L, Smith LB, Rebourcet D. Sertoli cells as key drivers of testis function. Semin Cell Dev Biol. 2022;121:2–9.
19. Cool J, DeFalco T, Capel B. Testis formation in the fetal mouse: dynamic and complex de novo tubulogenesis. Wiley Interdiscip Rev Dev Biol. 2012;1(6):847–59.
20. Rios-Rojas C, Spiller C, Bowles J, Koopman P. Germ cells influence cord formation and Leydig cell gene expression during mouse testis development. Dev Dyn. 2016;245(4):433–44.
21. Lee WY, Do JT, Park C, Kim JH, Chung HJ, Kim KW, et al. Identification of Putative Biomarkers for the Early Stage of Porcine Spermatogonial Stem Cells Using Next-Generation Sequencing. PLoS One. 2016;11(1):e0147298.
22. Lee R, Park HJ, Lee WY, Han MG, Park JH, Moon J, et al. Effect of Epidermal Growth Factor on the Colony-formation Ability of Porcine Spermatogonial Germ Cells. Biotechnology and Bioprocess Engineering. 2021;26(4):677–87.
23. Andrews S. FastQC: a quality control tool for high throughput sequence data. Cambridge, United Kingdom; 2010.
24. Dobin A, Davis CA, Schlesinger F, Drenkow J, Zaleski C, Jha S, et al. STAR: ultrafast universal RNA-seq aligner. Bioinformatics. 2013;29(1):15–21.
25. Anders S, Pyl PT, Huber W. HTSeq--a Python framework to work with high-throughput sequencing data. Bioinformatics. 2015;31(2):166–9.
26. Love MI, Huber W, Anders S. Moderated estimation of fold change and dispersion for RNA-seq data with DESeq2. Genome Biol. 2014;15(12):550.
27. Lee WY, Park HJ, Lee R, Lee KH, Kim YH, Ryu BY, et al. Establishment and in vitro culture of porcine spermatogonial germ cells in low temperature culture conditions. Stem Cell Res. 2013;11(3):1234–49.
28. Zhao X, Wan W, Li B, Zhang X, Zhang M, Wu Z, et al. Isolation and in vitro expansion of porcine spermatogonial stem cells. Reprod Domest Anim. 2022;57(2):210–20.
29. Sohni A, Tan K, Song HW, Burow D, de Rooij DG, Laurent L, et al. The Neonatal and Adult Human Testis Defined at the Single-Cell Level. Cell Rep. 2019;26(6):1501–17 e4.
30. Awang-Junaidi AH, Fayaz MA, Goldstein S, Honaramooz A. Using a testis regeneration model, FGF9, LIF, and SCF improve testis cord formation while RA enhances gonocyte survival. Cell Tissue Res. 2022;389(2):351–70.
31. Devi L, Pothana L, Goel S. Dysregulation of angiogenesis-specific signalling in adult testis results in xenograft degeneration. Sci Rep. 2017;7(1):2605.
32. Dabaja AA, Schlegel PN. Microdissection testicular sperm extraction: an update. Asian J Androl. 2013;15(1):35–9.
33. Dollet C, Shindo M, Takahashi S, Ito K, Eto T, Watanabe T. Germ cell depletion using HSV-TK in mouse testes. Sci Rep. 2025;15(1):9596.
34. Chen T, Wang Y, Tian L, Guo X, Xia J, Wang Z, et al. Aberrant Gene Expression Profiling in Men With Sertoli Cell-Only Syndrome. Front Immunol. 2022;13:821010.
35. Lee R, Lee WY, Park HJ, Ha WT, Woo JS, Chung HJ, et al. Stage-specific expression of DDX4 and c-kit at different developmental stages of the porcine testis. Anim Reprod Sci. 2018;190:18–26.
36. Zheng Y, Gao Q, Li T, Liu R, Cheng Z, Guo M, et al. Sertoli cell and spermatogonial development in pigs. J Anim Sci Biotechnol. 2022;13(1):45.
37. Davidova N, Jonakova V, Manaskova-Postlerova P. Expression and localization of acrosin inhibitor in boar reproductive tract. Cell Tissue Res. 2009;338(2):303–11.

ARTICLE IN PRESS

ARTICLE IN PRESS

38. Singh B, Singh R, Chaturvedi MM, Purohit JS. Sperm histone mediated epigenetic inheritancedagger. Biol Reprod. 2025;113(5):1061–82.
39. Armstrong JF, Pritchard-Jones K, Bickmore WA, Hastie ND, Bard JB. The expression of the Wilms' tumour gene, WT1, in the developing mammalian embryo. Mech Dev. 1993;40(1-2):85–97.
40. Wilhelm D, Englert C. The Wilms tumor suppressor WT1 regulates early gonad development by activation of Sf1. Genes Dev. 2002;16(14):1839–51.
41. Luo X, Ikeda Y, Parker KL. A cell-specific nuclear receptor is essential for adrenal and gonadal development and sexual differentiation. Cell. 1994;77(4):481–90.
42. Hossain A, Saunders GF. The human sex-determining gene SRY is a direct target of WT1. J Biol Chem. 2001;276(20):16817–23.
43. Miyamoto Y, Taniguchi H, Hamel F, Silversides DW, Viger RS. A GATA4/WT1 cooperation regulates transcription of genes required for mammalian sex determination and differentiation. BMC Mol Biol. 2008;9:44.
44. Irie N, Lee SM, Lorenzi V, Xu H, Chen J, Inoue M, et al. DMRT1 regulates human germline commitment. Nat Cell Biol. 2023;25(10):1439–52.
45. Hammes A, Guo JK, Lutsch G, Leheste JR, Landrock D, Ziegler U, et al. Two splice variants of the Wilms' tumor 1 gene have distinct functions during sex determination and nephron formation. Cell. 2001;106(3):319–29.
46. Ahmed SF, Bashamboo A, Lucas-Herald A, McElreavey K. Understanding the genetic aetiology in patients with XY DSD. Br Med Bull. 2013;106:67–89.
47. Koopman P, Gubbay J, Vivian N, Goodfellow P, Lovell-Badge R. Male development of chromosomally female mice transgenic for Sry. Nature. 1991;351(6322):117–21.
48. O'Shaughnessy PJ, Hu L, Baker PJ. Effect of germ cell depletion on levels of specific mRNA transcripts in mouse Sertoli cells and Leydig cells. Reproduction. 2008;135(6):839–50.
49. Gewiss RL, Law NC, Helsel AR, Shelden EA, Griswold MD. Two distinct Sertoli cell states are regulated via germ cell crosstalkdagger. Biol Reprod. 2021;105(6):1591–602.
50. Ohinata Y, Payer B, O'Carroll D, Ancelin K, Ono Y, Sano M, et al. Blimp1 is a critical determinant of the germ cell lineage in mice. Nature. 2005;436(7048):207–13.
51. Yamaji M, Seki Y, Kurimoto K, Yabuta Y, Yuasa M, Shigeta M, et al. Critical function of Prdm14 for the establishment of the germ cell lineage in mice. Nat Genet. 2008;40(8):1016–22.
52. Hersmus R, Kalfa N, de Leeuw B, Stoop H, Oosterhuis JW, de Krijger R, et al. FOXL2 and SOX9 as parameters of female and male gonadal differentiation in patients with various forms of disorders of sex development (DSD). J Pathol. 2008;215(1):31–8.
53. Matson CK, Murphy MW, Sarver AL, Griswold MD, Bardwell VJ, Zarkower D. DMRT1 prevents female reprogramming in the postnatal mammalian testis. Nature. 2011;476(7358):101–4.
54. Minkina A, Matson CK, Lindeman RE, Ghyselinck NB, Bardwell VJ, Zarkower D. DMRT1 protects male gonadal cells from retinoid-dependent sexual transdifferentiation. Dev Cell. 2014;29(5):511–20.
55. Wilhelm D, Washburn LL, Truong V, Fellous M, Eicher EM, Koopman P. Antagonism of the testis- and ovary-determining pathways during ovotestis development in mice. Mech Dev. 2009;126(5-6):324–36.
56. Zhang L, Guo M, Liu Z, Liu R, Zheng Y, Yu T, et al. Single-cell RNA-seq analysis of testicular somatic cell development in pigs. J Genet Genomics. 2022;49(11):1016–28.
57. Miles DC, Wakeling SI, Stringer JM, van den Bergen JA, Wilhelm D, Sinclair AH, et al. Signaling through the TGF Beta-Activin Receptors ALK4/5/7 Regulates Testis Formation and Male Germ Cell Development. PLOS ONE. 2013;8(1):e54606.
58. Sasaki K, Yokobayashi S, Nakamura T, Okamoto I, Yabuta Y, Kurimoto K, et al. Robust In Vitro Induction of Human Germ Cell Fate from Pluripotent Stem Cells. Cell Stem Cell. 2015;17(2):178–94.
59. Kim Y, Kobayashi A, Sekido R, DiNapoli L, Brennan J, Chaboissier MC, et al. Fgf9 and Wnt4 act as antagonistic signals to regulate mammalian sex determination. PLoS Biol. 2006;4(6):e187.

ARTICLE IN PRESS

ARTICLE IN PRESS

815

816

817

818

819

820

821

822

823

824

825

826

827

828

829

830

831

832

ARTICLE IN PRESS

ARTICLE IN PRESS

Figure captions

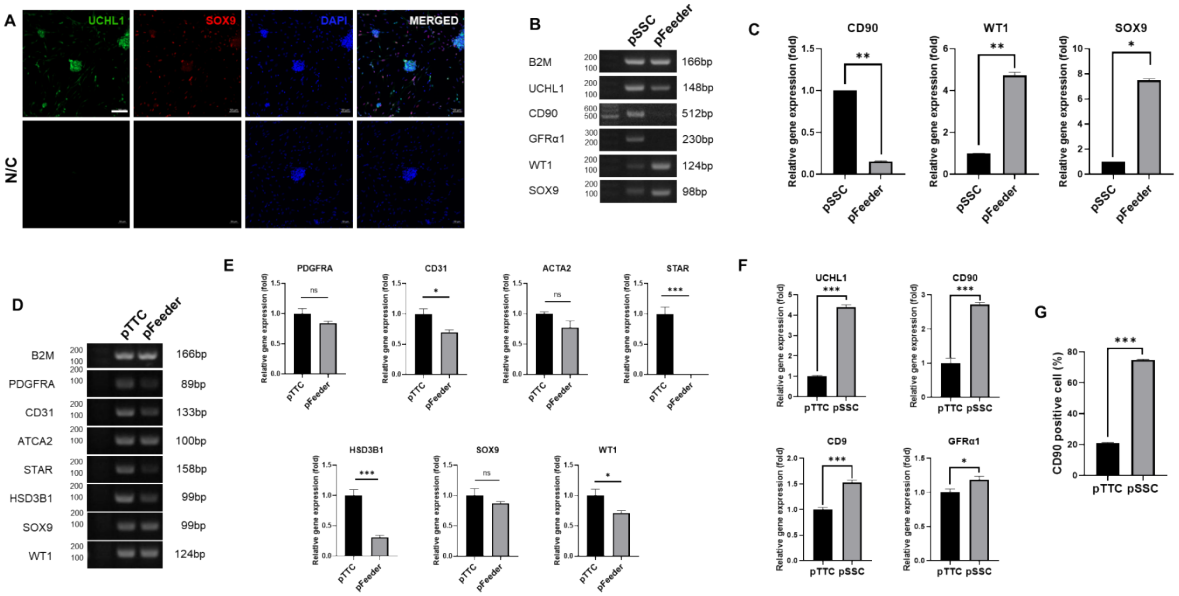

Fig. 1. Characterization of porcine spermatogonial stem cells (pSSCs) and porcine testicular somatic-enriched fraction (SEF) feeder cells. (a) Protein expression of UCHL1 (green), SOX9 (red), and DAPI in pSSCs colony and SEF feeder cells (N/C, negative control; scale bar = 100 μm). **(b)** Expression of specific markers in spermatogonia and Sertoli cells was assessed using RT-PCR. **(c)** Relative gene expression levels of *CD90*, *WT1*, and *SOX9* between pSSC colony and SEF feeder cells. **(d)** testicular somatic cell-related gene expression of porcine total testicular cells (pTTCs) and SEF feeder cells **(e)** spermatogonia stem cell-related gene expression of pTTCs and pSSC colony. **(f)** CD90-positive population of pTTC and pSSC colony. The housekeeping gene *B2M* was used as a control. Full-length gels are presented in Additional file 1. Graphs represent the mean ± standard error (* $p < 0.05$, ** $p < 0.01$, *** $p < 0.001$).

ARTICLE IN PRESS

ARTICLE IN PRESS

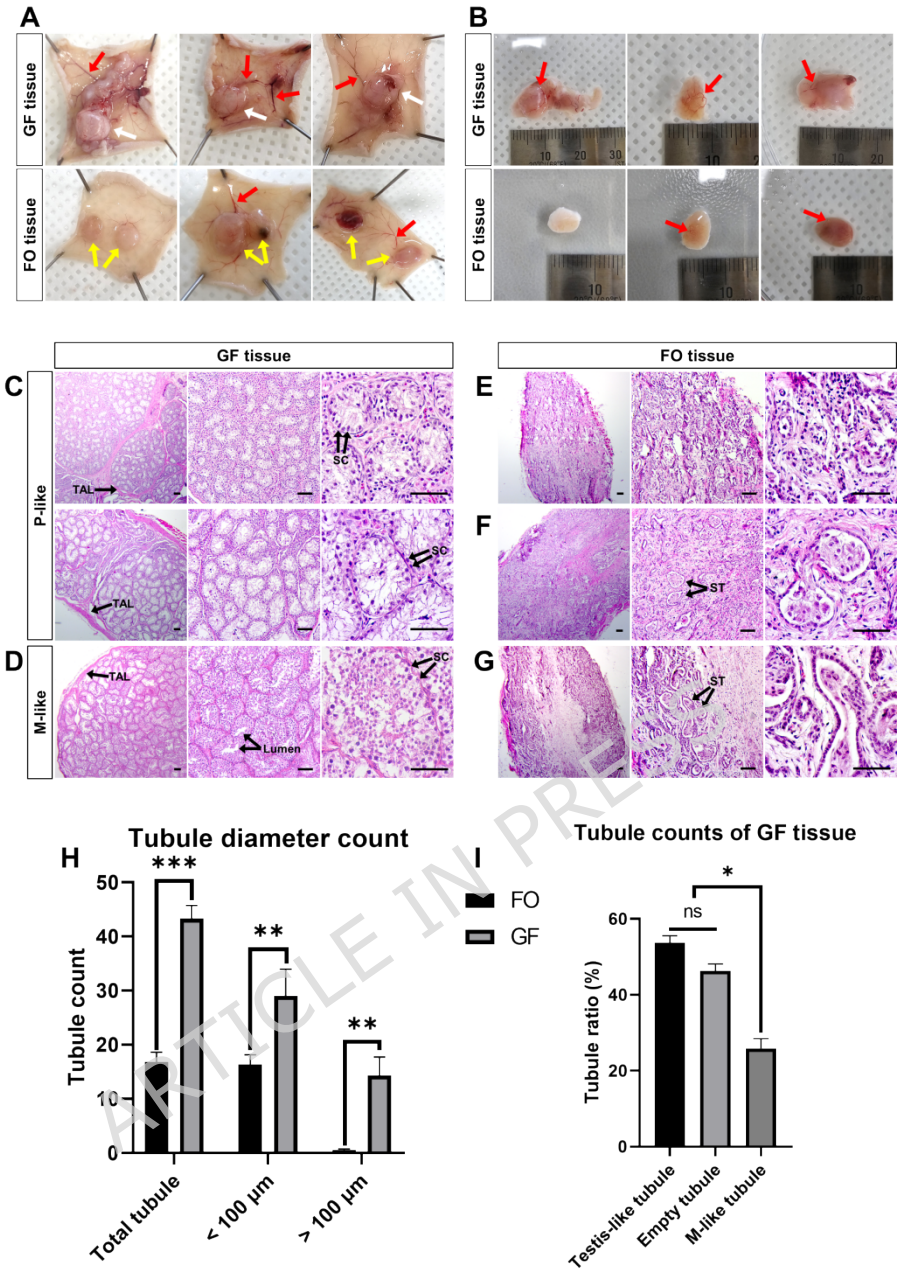

Fig. 2. Formation and histological characterization of tissues from xenografted porcine testicular cells. (a) Tissues derived from pSSC enriched germ cells and SEF (GF tissue) and SEF only (FO tissue). White and yellow arrows indicate tissues, while red arrows indicate blood vessels. **(b)** Washed reconstitute tissues isolated from mouse skin. **(c–d)** Hematoxylin and eosin (H&E) stained sections from the testis-like structures of GF tissues (P-like, prepubertal-like; M-like, mature-like; TAL, tunica albuginea-like structure; SC, Sertoli cells; scale bar = 100 µm). **(e–g)** H&E-stained sections from FO tissue structures (ST: simple tubule; scale bar = 100 µm). **(h)** tubule count of GF and FO tissue (n = 3

ARTICLE IN PRESS

per section). **(i)** percentage of testis-like, empty and M-like tubules of GF tissue (n = 3 per section). Graphs represent the mean ± standard error (** $p < 0.01$, *** $p < 0.001$).

.

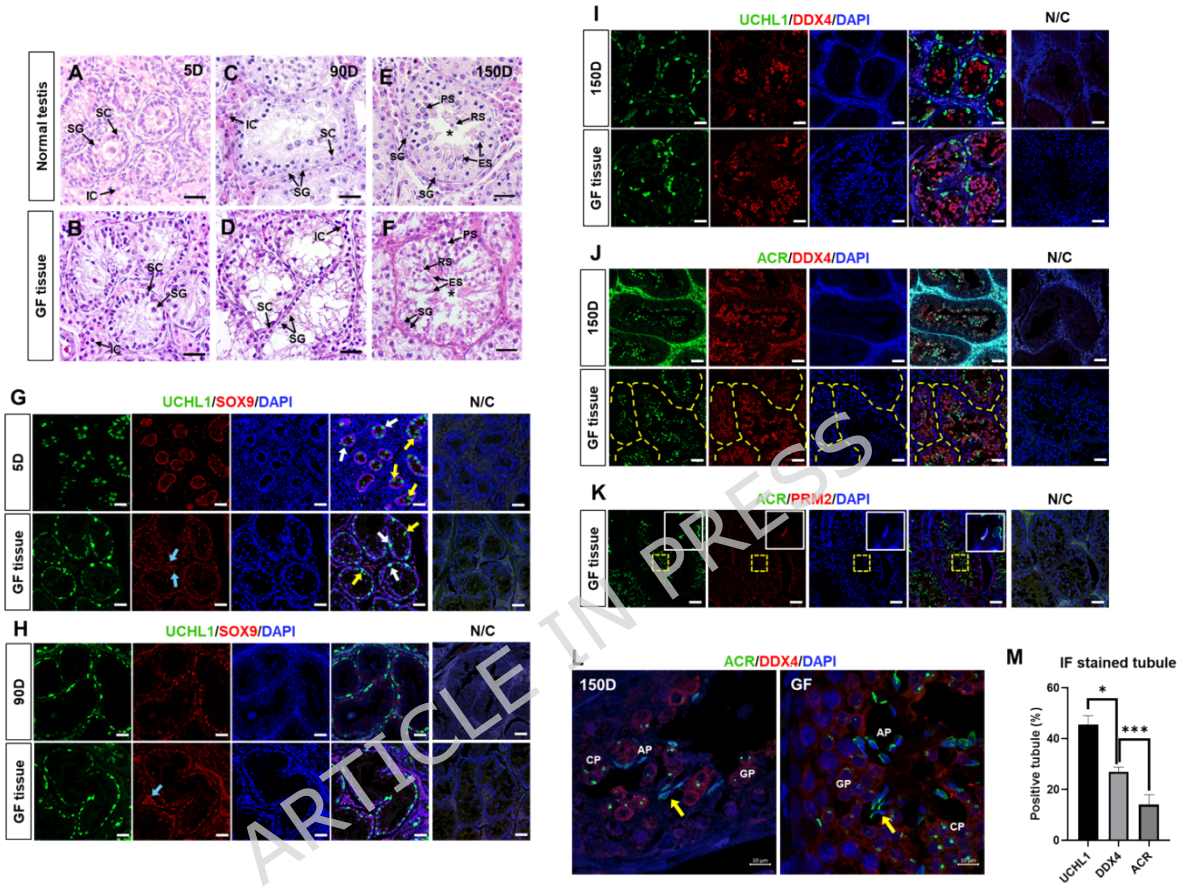

ARTICLE IN PRESS

Fig. 3. Histological comparison of the normal testes and reconstituted GF tissues. (a), (c), (e) Hematoxylin and eosin (H&E) staining of normal testes (5-d-old: 5D, 90-d-old: 90D, and 150-d-old: 150D). **(b), (d), (f)** GF tissues containing spermatogonia in the tubules (GF, tissues composed of pSSC enriched germ cells and SEF; SG, spermatogonia; SC, Sertoli cells; IC, interstitial cells; PS, primary spermatocyte; RS, round spermatid; ES, elongated spermatid; * = center of lumen; scale bar = 100 μm). **(g)** Staining for UCHL1, SOX9 in 5D and GF tissues (N/C, negative control; scale bar = 40 μm). White arrows indicate SG in the basement membrane, and yellow arrows indicate SG in the seminal cord. Blue arrows indicate SOX9-positive cells in the interstitial area. **(h)** Staining for UCHL1 and SOX9 in 90D and GF tissues (scale bar = 40 μm). Blue arrows indicate SOX9-positive cells in the interstitial area. **(i)**

ARTICLE IN PRESS

Visualization of UCHL1 and DDX4 protein expression from 150D testes and GF tissues (scale bar = 40 μm). **(j)** Immunohistochemistry (IHC) for ACR and DDX4 in the 150D testes and GF tissues. The line represents the outline of the tubules in GF tissue (scale bar = 40 μm). **(k)** Protamine2 (PRM2) expression of GF tissue (scale bar = 40 μm). **(l)** Detailed views of ACR and DDX4 expression in 150D testes and GF tissues. Yellow arrows indicate elongated spermatids (GP, Golgi phase; CP, cap phase; AP, acrosome phase; scale bar = 10 μm). **(m)** Percentage of UCHL1, DDX4, and ACR positive tubules in GF tissue (n = 3, * $p < 0.05$, *** $p < 0.001$).

ARTICLE IN PRESS

ARTICLE IN PRESS

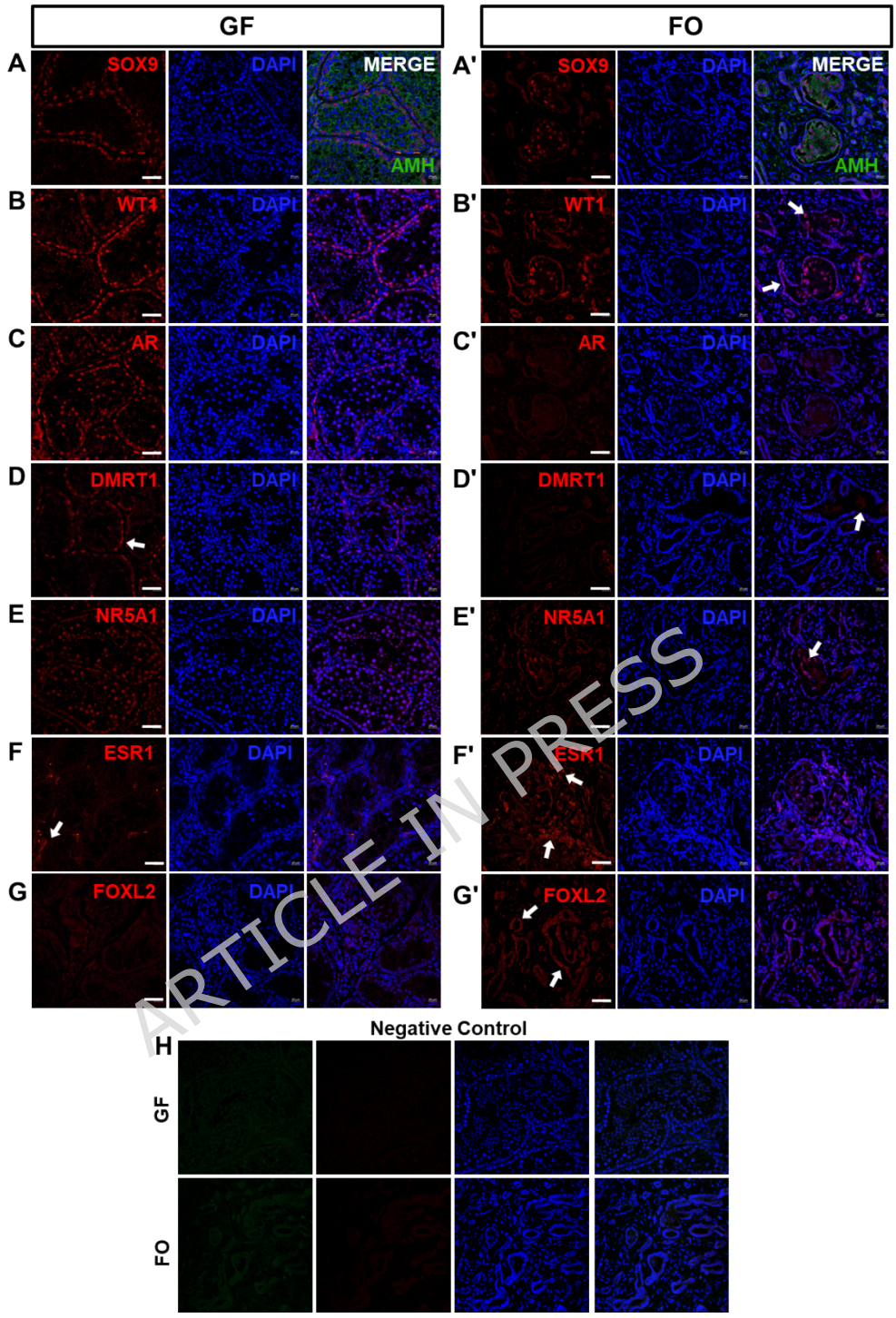

877

878 **Fig. 4. Examination of Sertoli cell-related protein expression in GF and FO tissues. (a)** Staining for

879 AMH and SOX9 in GF and FO tissues (GF, pSSC enriched germ cells and SEF; FO, tissues of SEF only

880 with lacking germ cells; scale bar = 40 μm). **(b-e)** Staining for WT1, AR, DMRT1, and NR5A1 (also

881 known as SF-1) in GF and FO tissues (scale bar = 40 μm). **(f) (g)** Staining for ESR1 and FOXL2 in GF

882 and FO tissues. All white arrows indicate staining-positive cells. **(h)** Negative control staining of GF

ARTICLE IN PRESS

and FO tissue.

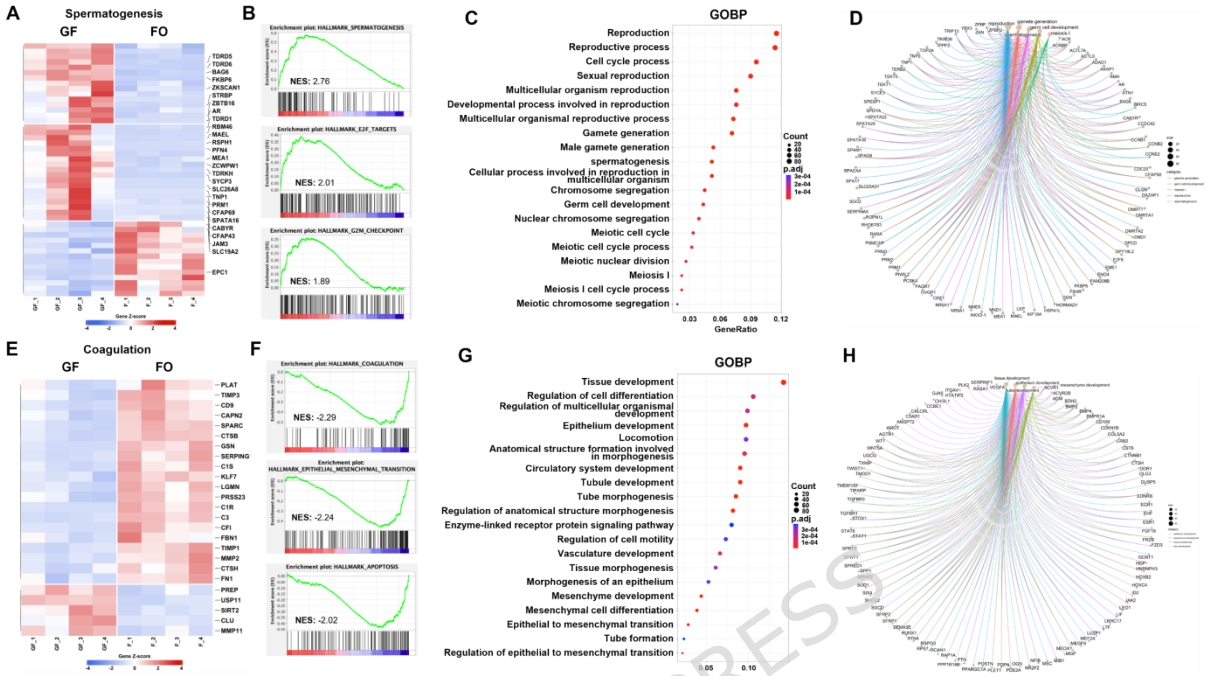

Fig. 5. RNA profiling of GF and FO tissues. The significant upregulation genes in GF and FO tissue (GF, pSSC enriched germ cells and SEF; FO, tissues of SEF only with lacking germ cells) were further analyzed using the Database for Annotation, Visualization, and Integrated Discovery (DAVID) for Gene Ontology Biological Processes (GOBP). **(a)** Heatmap of differential expression genes (DEGs) associated with spermatogenesis. **(b)** Gene Set Enrichment Analysis (GSEA) of total DEGs in GF tissues with normalized enrichment score (NES) scores. NES scores were 2.76, 2.01, and 1.89 for spermatogenesis, E2F targets, and G2M checkpoint, respectively. **(c)** Dot plot representing GOBP analysis of genes upregulated in GF tissues. **(d)** CNET plot showing spermatogenesis-related GOBP and gene expression in GF tissue. **(e)** Heatmap of DEGs associated coagulation. **(f)** GSEA of total DEGs in FO tissues with NES scores. NES scores were -2.29, -2.24, and -2.02 for coagulation, epithelial-mesenchymal transition, and apoptosis respectively. **(g)** Dot plot representing GOBP analysis of the upregulated genes in FO tissues. **(h)** CNET plot illustrating tissue development-related GOBP and the interaction of upregulated genes in the FO tissue.

ARTICLE IN PRESS

ARTICLE IN PRESS

900

901

902

903

ARTICLE IN PRESS

ARTICLE IN PRESS

Additional files

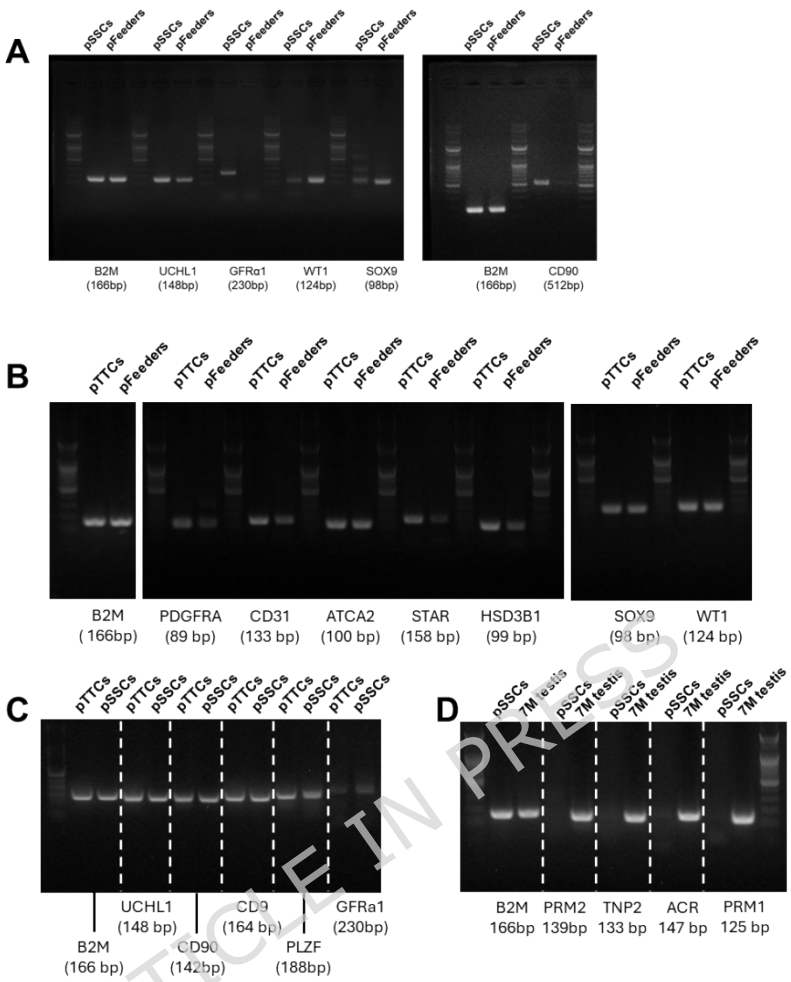

Additional file 1. Uncropped image of full-length gels RT-PCR and qPCR. This file contains uncropped images of gel electrophoresis for PCR products. (a) Uncropped gel image of Figure 1b. (b) Uncropped gel image of qPCR of Figure 1d. (c) Uncropped gel image of qPCR of Figure 1e. (d) further validation of PRM1, PRM2, TNP2 and ACR expression of pSSC colony and 7-month old testis.

Supplementary table 1. Primer list of spermatogenesis-related genes in additional file 1.

Gene (RT-PCR)	Primer sequence
PLZF (188 bp)	F: GGCTCGGTATCTCAAGAACATC R: ACTGCCCTATGGTCATCAAACT
PRM1 (125 bp)	F: CCGCCGCTACACCGTTATA R: CAGTAGTGGCATGTTCAAGATG

ARTICLE IN PRESS

PRM2 (139 bp)	F: GGGCCGCTACCACTACAGAC R: GCCTCCTTCTGCATCTTCTC
TNP2 (133 bp)	F: CACCAAGGCATCGCAAAC R: GCTCCTCTTGATTCCCTTCC
ACR (147 bp)	F: ACCTGGCCCTATCTGAACTG R: AGTACCAAGGTGGGCGAAC

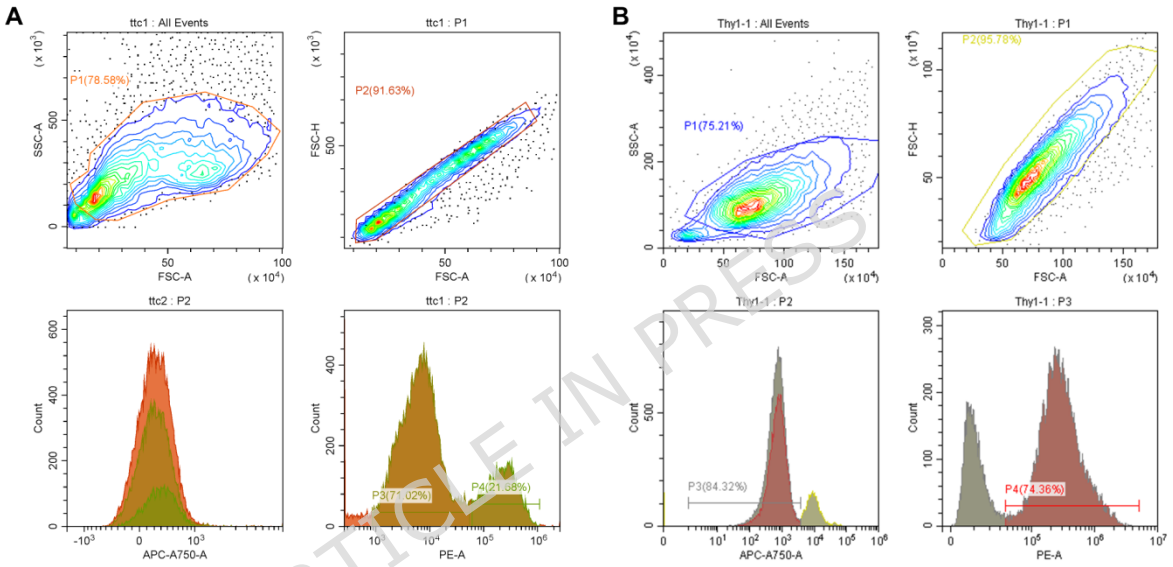

Additional file 2. Gating strategy of flowcytometry of pTTC and pSSC colony. Raw data and gating strategy of CD90 (THY1) protein expression of (a) porcine testis total cells (pTTC) and (b) pSSC colony for Figure 1f.

ARTICLE IN PRESS

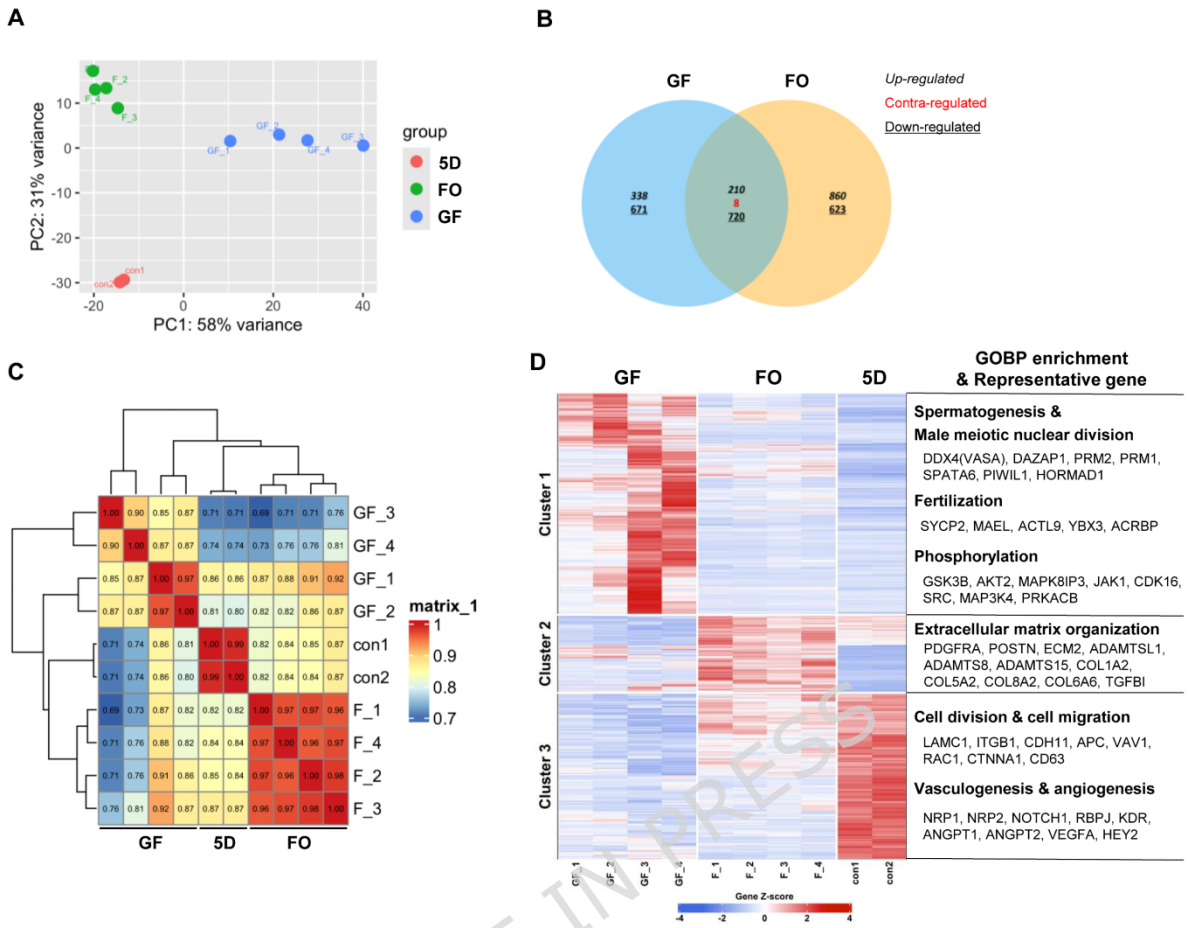

Additional file 3. DEG profiling among 5-d-old testes, GF and FO tissues. This file details the differentially expressed gene (DEG) profiling among 5-d-old (5D) testes, GF, and FO tissues (GF, pSSC enriched germ cells and SEF; FO, tissues of SEF only with lacking germ cells). **(A)** Principal component analysis (PCA) of 5D testis, GF, and FO tissues. **(B)** Venn diagram between GF and FO tissues compared to 5D testis. **(C)** Correlation plot of 5D testis, GF, and FO tissues. **(D)** Heatmap illustrating terms of enriched GOBP and representative genes of Gene Ontology Biological Processes (GOBP) in 5D testis, GF, and FO tissues.

ARTICLE IN PRESS